Nanoscale

Accepted Manuscript

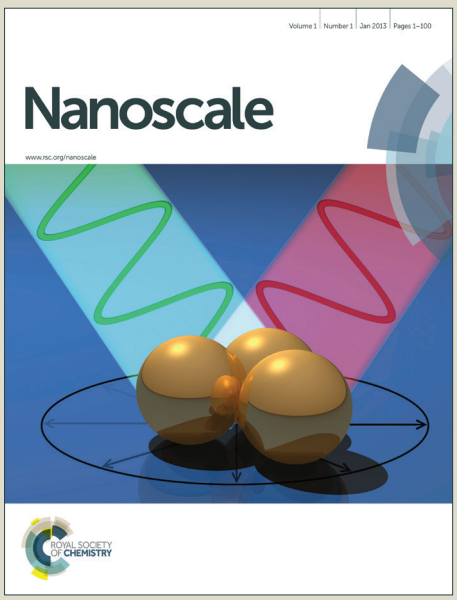

ROYAL SOCIETY OF CHEMISTRY

www.rsc.org/nanoscale

Thermal Conductivity of Twisted Bilayer Graphene

Hongyang Li,[a] Hao Ying,[a] Xiangping Chen,[a] Denis L. Nika,[b,c] Alexandr I. Cocemasov,[c] Weiwei Cai,[a] Alexander A. Balandin[*b] and Shanshan Chen[*a]

We have investigated experimentally the thermal conductivity of suspended twisted bilayer graphene. The measurements were performed using the optothermal Raman technique. It was found that the thermal conductivity of the twisted bilayer graphene is lower than that of monolayer graphene and the reference Bernal stacked bilayer graphene in the entire examined temperature range (~300 K – 700 K). This finding indicates that the heat carriers – phonons – in the twisted bilayer graphene do not behave themselves as in individual graphene layers. The decrease in the thermal conductivity in twisted bilayer graphene was explained by the modification of the Brillouin zone due to plane rotation and emergence of numerous folded phonon branches that enhance the phonon Umklapp and normal scattering. The obtained results are important for understanding thermal transport in two-dimensional systems.

1. Introduction

The discovery of the unusually high thermal conductivity, K, of graphene[1-3] and the unique nature of K value scaling with the thickness in suspended few-layer graphene (FLG)[4] stimulated a large body of follow up experiments[5-9] and theoretical investigations.[10-15] It has been shown that the high thermal conductivity of graphene is related to specifics of the long-wavelength phonon transport in two-dimensional (2-D) systems. The logarithmic divergence of K in 2-D crystalline lattice of graphene predicted using different model assumptions[3, 14]has been confirmed experimentally.[16] The experimental observation of the increased intrinsic K in FLG with reduction of the number of atomic planes has been supported by numerous theoretical calculations.[3, 14, 15] The rapidly developing graphene has now entered the domain of applications with the reports of graphene use in thermal interface materials,[17] thermal phase change materials18 and heat spreaders.[19-21]

One of the remaining important questions of phonon thermal transport in graphene is how the thermal conductivity is affected by rotating the atomic planes in twisted bilayer graphene (T-BLG). The answer to this question has both fundamental science and practical implications. It was predicted theoretically that the low-energy electron dispersion in T-BLG is linear as in a single layer graphene (SLG).[22-24] Independent studies suggested that electrons in T-BLG behave like massless Fermions either with the same[22, 23] or somewhat reduced Fermi velocity.[24] Most of the theoretical predictions for electron transport in T-BLG have been confirmed experimentally.[25-27] In this paper we pose a crucial question: do acoustic phonons – the main heat carriers in graphene – also behave in T-BLG as phonons in SLG? If yes, one can envision extraordinary heat fluxes via stacks of FLG with the atomic plans rotated with respect to each other. If no, what mechanism would suppress the heat conduction in the weakly bound twisted atomic plane? From the practical point of view, it is also interesting to compare the heat conduction properties of conventional BLG with those of T-BLG.

2. Results and discussion

The high-quality multilayer graphene films were synthesized by the chemical vapor deposition (CVD) on the outside surface of the Cu foil enclosures with a methane flow rate of 5 sccm and a partial pressure of 75 mTorr at

1030□.[28] For grapheme transfer, the graphene-on-Cu sample was spin coated with poly-methyl methacrylate (PMMA) that was then cured.[29] After the Cu substrate was dissolved in an $(NH_4)S_2O_8$ solution (0.3M), the PMMA-graphene film was transferred to the SiO_2/Si substrate or SiN_x substrates. After the PMMA was removed using acetone, graphene on the SiO_2/Si substrate or the suspended graphene on the SiN_x substrate were dried in vacuum (pressure 5×10^{-8}Torr) to further remove the adsorbate as well as to make a better contact between graphene and the substrates. Before the thermal measurements, micro-Raman (WITec Alpha-300) spectroscopy was used to determine the number of atomic planes and the stacking order in FLG samples. A typical optical image of as-synthesized graphene transferred on SiO_2/Si substrate is shown in Figure 1 (a). The variation of color contrast in the optical image indicates the presence of two BLG domains.[30] Raman spectra accumulated at the position of the color circles in Figure 1 (a) are shown in Figure 1 (b). The spectrum from the domain marked by the blue circle in Figure 1 (a) shows a typical Bernal (AB) BLG feature with slightly higher G band than 2D band and a full width at half maximum (FWHM) of the 2D band of ~50 cm^{-1}. The spectrum from the domain, marked by the green circle, shows features similar to SLG, which suggest a rotationally twisted order of the BLG. The Raman mapping of BLG samples were shown in Figure 1 (c) where the bright region in the G intensity map demonstrate the uniformity of the two BLG domains. Furthermore, the bright regions in the 2D intensity map and 2D FWHM map suggest that the stacking order of the upper and lower domains are the Bernal and rotationally faulted, also referred to as twisted, respectively.

In order to perform the non-contact thermal measurements using the optothermal Raman technique[1, 3], we transferred a different portion of the same BLG on the Au-coated silicon nitride (SiNx) membrane with a pre-fabricated 100×100 array of 2.8 μm diameter holes. Figure 2 (a) shows a representative mapping of the Raman 2D intensity acquired over a 30×30 μm^2 area. The Raman data shows the presence of the graphene suspended on the holes. In Figure 2 (b) we present Raman spectra taken from three selected holes marked by the arrows in Figure 2 (a). The one marked by the red arrow shows SLG features with the well-defined 2D/G intensity ratio. The graphene film over the hole marked by the blue arrow shows typical AB-BLG features with much larger FWHM of the 2D band. The T-BLG graphene sample marked by the green arrow is recognized from the intensity of the G peak similar to AB-BLG but with much narrower FWHM of the 2D band.[31, 32] The disorder D band for the graphene samples is either absent or very weak attesting to the high quality of CVD graphene.

Since the knowledge of the number of atomic planes and stacking order is essential for the present study, we verified the Raman data with the electron diffraction, transmission electron microscopy (TEM) and selective area electron diffraction (SAED) measurements. The TEM inspection was performed after the thermal measurements to avoid damage to the graphene samples. Figures 2 (c-d) presents diffraction patterns with the 6-fold symmetry detected on the SLG and AB-BLG samples. Alternatively, two set of 6-fold diffraction patterns were found on the T-BLG region. The corresponding diffraction peak intensities along the red and violet lines are shown in Figure 2 (f-h). In Figure 2 (f) the intensity of the first-order diffraction is higher than that of the second-order indicating SLG.[33] Although the diffraction patterns have the same orientation as those of SLG the first-order diffraction in

Figure 2 (g) has a lower intensity than the second-order suggesting that BLG is AB-stacked.[33] The diffraction pattern of T-BLG which is determined to have the rotation angle of approximately 34° is shown in Figure 2 (e). We also plotted the diffraction peak intensities along AA' and BB' in Figure 2(h) indicating each set of reflections resulting from the individual graphene layers. At this stage, the controllable synthesis of BLG by CVD is still of great challenge, especially for the regulating of twist angle of T-BLG[34]. The rotation angle of ~34° is chosen to match the commensurate crystal structures used for the theoretical analysis described below.

The optical transmission or absorption of the suspended graphene samples is required for the optothermal measurements of the thermal conductivity.[1] In the present work, the optical transmission through the center of the suspended graphene was measured using a semiconductor laser power meter (Newport 1918-c) placed under the SiNx support.[5] The measured optical absorption for one path through SLG was 3.4±0.67% at 488 nm wavelength, which is comparable to the literature values.[5, 6, 35] The FLG transparency decreases with increasing numbers of the atomic planes.[36] The measured optical absorption of BLG was 6.8±0.72% for the Bernal stacked AB-BLG domains and 6.9±0.70% for T-BLG.

In order to investigate phonon transport and heat conduction in the suspended SLG, AB-BLG, and T-BLG samples we adopted the optothermal Raman technique.[1, 3-6, 36] The technique used temperature dependence of the G peak and 2D band in Raman spectrum of graphene for extraction of the temperature rise, ΔT, in response to local heating with the laser.[1, 3] The knowledge of the absorbed power together with ΔT and geometry of the suspended samples allows one to extract K value via solution of the heat-diffusion equation.[3-6] The relatively large size of the samples ensures that the phonon transport is in the diffusive or partially diffusive regime. Considering that the average phonon MFP in graphene is ~775 nm[3], the phonons will undergo a couple of scattering events before reaching the edge of the hole. Details of the method and thermal data extraction have been reported by some of us elsewhere.[1, 3-6]

For these measurements, we focused the 488-nm laser beam on the sample using a 100× objective lens. The laser spot was focused on the center of the suspended graphene and the laser power was set for ten values ranged from 0.1 mW to 10 mW. The temperature rise in the optically heated graphene causes a red shift of the 2D peak, which can be used for the local temperature measurement. The relationship between the 2D peak shift and the graphene temperature was established via the calibration measurements by collecting Raman spectrum under low excitation power of the graphene sample placed on a heating stage with its temperature determined with a thermocouple.6 Figure 3 presents the results of the calibration measurements for all three types of samples. The Raman 2D peak of SLG (red triangles) down shifts with increasing stage temperature at a rate of $(5.9\pm0.7)\times10^{-2}$ cm^{-1}/K. The temperature coefficients for T-BLG (green circles) and AB-BLG (blue triangles) were determined to be $(3.1\pm0.2)\times10^{-2}$ cm^{-1}/K and $(3.4\pm0.4)\times10^{-2}$ cm^{-1}/K, respectively.

For the thermal data extraction we ignored heat loss via radiation owing to the small size of the sample and fast measurement procedure. The measured thermal resistance of the graphene sample is defined as $R_m \equiv \frac{T_m - T_0}{Q_{ab}}$, where T_m is the temperature rise determined by the 2D peak shift obtained in the centre of each suspended graphene

membrane, T_o is the substrate temperature of 300K, and Q_{ab} is the absorbed laser power through the suspended graphene layer, which is defined by the laser power on the sample and its optical absorption. Moreover, R_m contains a thermal contact resistance R_c between the graphene region and the Au/SiN_x support and a thermal resistance from the suspended graphene R_g. Based on the same sample geometry and analysis methods with our previous work, the R_c is one order smaller than the measured thermal resistance of the graphene sample, which is attributed to the large contact area achieved in the radial heat flow geometry compared to an axial heat flow pattern[5, 6, 9, 37] For the case of the phonon transport is diffusive in the suspended graphene region and that the laser beam is focused on the centre of each suspended graphene membrane, the thermal conductivity was calculated as[5]

$$K = \frac{\ln(R/r_0)}{2\pi t R_g}\alpha \quad (1)$$

where R=1.4 μm is the radius of the holes; t is the graphene monolayer thickness, and r_0 is the radius of the Gaussian laser beam. The radius of the laser beam spot r_0 was determined by performing micro-Raman scans across a smooth cleaved edge of a Si substrate.[5] Based on the models discussed in our previous work,[5] the r_0 value is of 0.158μm and the α factor accounts for the Gaussian beam profile is calculated as 0.98 for the 100× objective lens on our Raman system. The large lateral dimensions of the graphene flakes supported by metal ensure a good thermal contact and ideality of the heat sink.

Figure 4 shows thermal conductivity K as a function of the measurement temperature T_m for SLG, AB-BLG and T-BLG, respectively. The experimental uncertainty accounted for in the error bars include the Raman peak position temperature calibration, the temperature resolution of the Raman measurement method and the uncertainty of the measured laser absorption.[6] The thermal conductivity of SLG at 310 K is 2778 ± 569W/mK. This value is above bulk graphite and it is close to those reported in previous studies.[3, 5, 6, 37] One should also keep in mind that K of suspended SLG depends on the size of the sample owing to the exceptionally large mean free path (MFP) of the long-wavelength phonons in graphene.3 The thermal conductivity of AB-BLG and T-BLG are 1896 ± 410 W/mK at 314 K and 1413 ± 390 W/mK at 323 K, respectively. Due to the specific of the experimental technique the results are given at similar but not exactly the same measurement temperature T_m. For comparison, Figure 4 also provides data for wrinkled SLG from Ref. (9).

The first observation from the experimental data is that the phonon thermal conductivity decreases over the entire temperature range as one goes from SLG to AB-BLG and, then, to T-BLG. The K value of wrinkled SLG is between that of SLG and AB-BLG. The result that K of suspended SLG is substantially larger than that of the suspended BLG is consistent with the previous reports.[3, 4] It has been explained theoretically by the increase in the phase space available for the phonon Umklapp scattering in BLG as compared to that in SLG.[4] The same conclusion about the lower intrinsic thermal conductivity of BLG as compared to SLG was reached on the basis of numerous independent MD simulation reports.[3, 14, 15] In this sense, our experimental data for SLG and AB-BLG are in line with previous studies.

The thermal conductivity of T-BLG is noticeably lower than that of AB-BLG over the entire examined temperature range. This trend is seen despite the relatively large experimental uncertainty of the measurement technique. All

data points for T-BLG were consistently below the data points for AB-BLG. Combined with the theoretical considerations given below, the experimental data indicate that the thermal conductivity of T-BLG is lower than that of AB-BLG for the examined twist angle and temperature range. While optothermal technique has relatively large systematic error due to finite spectral resolution of Raman spectrometers it avoids large experimental uncertainty associated with sample contamination and damage during nanofabrication required for other thermal measurement techniques[3]. The further analysis of the experimental data suggest that K of T-BLG deviates stronger from the 1/T dependence characteristic for the phonon transport limited by the phonon Umklapp scattering arising from inharmonicity of crystal lattice. The lower thermal conductivity of T-BLG means that the transport of acoustic phonons in the twisted atomic planes is not similar to that of electrons.[22-24] Unlike electrons, phonons do not propagate in T-BLG as in two nearly independent SLG planes despite the weakness of van der Waals interactions between the atomic planes of T-BLG.

In order to further rationalize the experimental results we plotted the Brillouin zones (BZ) for AB-BLG and T-BLG and calculated phonon dispersions in both cases. The theoretical analysis can only be performed for commensurate T-BLG structures, i.e. structures with translation symmetry. Such structures exist for certain rotational angles determined by the following condition[38]:$cos\,\theta(p,n) = (3p^2 + 3pn + n^2/2)/(3p^2 + 3pn + n^2)$, where p and n are co-prime positive integer numbers. If n is not divisible by 3, the number of atoms in T-BLG unit cell is given by a simpler equation[39]:$N = 4((p+n)^2 + p(2p+n))$. The unit cells of T-BLG with larger indices *(p,n)* contain a larger number of carbon atoms. For our analysis we selected the indices to ensure the commensurate structure and resulting in a twist angle 32.2°, which is close to the experimentally determined angle of ~34°. In order to construct BZ of T-BLG with the rotation angle $\theta(p,n)$ we determined the corresponding reciprocal vectors $\vec{g}_1$ and $\vec{g}_2$ of T-BLG (see Figure 5). The size of BZ in T-BLG depends on the rotation angle. The calculations of the phonon dispersion were performed using the Born-von Karman model of lattice dynamics for intra-layer atomic interactions and spherically symmetric interatomic potential for interlayer interactions. Details of our calculation procedures for phonon dispersion in T-BLG were reported by some of us earlier.[39, 40]

One can see in Figure 5 that twisting the atomic planes in BLG results in substantially reduced size of BZ and emergence of numerous folded acoustic phonon branches. The appearance of folded phonons and their dispersion relations have more to do with the symmetry breaking of AB stacking rather than changes in the van der Waals interactions. The modification of the phonon spectrum is somewhat similar to zone folding in conventional quantum well superlattices, which results in the on-set of mini-Umklapp scattering processes. The two-phonon scattering processes do not limit the thermal transport because they do not change the total momentum of the phonon system.[41] The intrinsic thermal conductivity is determined by the three-phonon scattering processes. The energy and momentum conservation laws for the three-phonon scatterings are written as follows:

$$\omega = \omega'' \pm \omega'$$
$$\vec{q} = \vec{q}'' \pm \vec{q}' \mp \vec{g} \qquad (2)$$

where $\vec{g} \neq 0$ is one of the vectors of the reciprocal lattices in the case of Umklapp scattering processes and $\vec{g} = 0$ for the normal scattering processes. The upper sign in Eq. (2) corresponds to the decay of phonon $\omega(\vec{q})$ into two phonons $\omega'(\vec{q}')$ and $\omega''(\vec{q}'')$ while the lower sign corresponds to the case when a phonon $\omega(\vec{q})$ absorbs a phonon $\omega'(\vec{q}')$ forming a phonon$\omega''(\vec{q}'')$.

In most bulk materials, the normal processes do not directly change the total momentum of the phonon system although they contribute to the thermal resistance by redistributing the population of the phonon modes. The main scattering mechanism limiting the heat conduction in bulk crystals is the three-phonon Umklapp scattering.[41] In low dimensional materials, the three-phonon normal scattering can affect the thermal conductivity stronger owing to strong non-linearity of the phonon dispersion and emergence of numerous confined branches.

There have been theoretical suggestions that normal phonon processes are more important in graphene than in bulk.[10, 42, 43] Calculation of the three-phonon scattering in graphene and FLG to the second order has shown explicitly how normal processes are limiting of the low-energy phonon MFP.[43] The Umklapp and normal scattering processes in T-BLG should also depend on the twist angle. The momentum of the phonon modes in T-BLG differs from that in BLG due to the twist. The latter opens up new channels for the phonon relaxation in T-BLG. The example of a new channel for phonon scattering is shown in Figure 5 (b, d): the normal decay of the phonon with $\omega = 900cm^{-1}$ (blue point) into two phonons with $\omega' = 800cm^{-1}$ and $\omega'' = 100cm^{-1}$ (green points). This scattering process is allowed by the momentum conservation law in T-BLG ($\vec{q} = \overrightarrow{q''} + \overrightarrow{q'}$) but it is not allowed in AB-BLG ($\vec{q} \ll \overrightarrow{q''} + \overrightarrow{q'}$). There are other scattering channels available in T-BLG, which are forbidden in AB-BLG by the momentum conservation laws. These considerations explain the lower thermal conductivity of T-BLG as compared to AB-BLG.

Conclusions

The near RT thermal conductivity of the suspended twisted bilayer graphene, K= 1412.8 ± 390 W/mK was found to be lower than that of AB stacked bilayer graphene, K=1896.2 ± 410 W/mK. The corresponding value for the single layer graphene was 2778.3 ± 569 W/mK in line with the previous reports. Our results prove that the phonon transport in T-BLG is substantially different from that of electrons. Phonons do not propagate in T-BLG as in two nearly independent SLG planes. The reduction of the thermal conductivity in T-BLG was explained by modification of the phonon dispersion resulting in the on-set of additional mini-Umklapp scattering channels for phonons.

Acknowledgements

Thanks to the discussion from Prof. Yong Zhang. We appreciate the support from the National Natural Science Foundation of China through grant Nos. 51302233, 11374244 and 11335006, and the Specialized Research Fund of the Doctoral Program of Higher Education (SRFDP, 20130121120017). AAB acknowledges support by the National Science Foundation via grant ECCS-1307671: Two Dimensional Performance with Three Dimensional

Capacity: Engineering the Thermal Properties of Graphene. DLN and AIC acknowledge support from the Moldova State Project 14.819.16.02F and STCU grant 5937.

Notes and references

[a]Department of Physics, Laboratory of Nanoscale Condense Matter Physics and State Key Laboratory of Physical Chemistry of Solid Surfaces, Xiamen University, Xiamen, 361005 China. E-mail: sschen@xmu.edu.cn

[b]Nano-Device Laboratory, Department of Electrical Engineering and Materials Science and Engineering Program, University of California – Riverside, Riverside, California, 92521 USA. E-mail: balandin@ee.ucr.edu

[c]E. Pokatilov Laboratory of Physics and Engineering of Nanomaterials, Department of Physics and Engineering, Moldova State University, Chisinau, MD-2009, Republic of Moldova.

1. A. A. Balandin, S. Ghosh, W. Bao, I. Calizo, D. Teweldebrhan, F. Miao and C. N. Lau, *Nano Lett.*, 2008, **8**, 902-907.

2. D. L. Nika, E. P. Pokatilov, A. S. Askerov and A. A. Balandin, *Phys. Rev. B*, 2009, **79**, 155413.

3. A. A. Balandin, *Nat. Mater.* 2011, **10**, 569-581.

4. S. Ghosh, W. Z. Bao, D. L. Nika, S. Subrina, E. P. Pokatilov, C. N. Lau and A. A. Balandin, *Nat. Mater.* 2010, **9**, 555-558.

5. W. W. Cai, A. L. Moore, Y. W. Zhu, X. S. Li, S. S. Chen, L. Shi and R. S. Ruoff, *Nano Lett.*, 2010, **10**, 1645-1651.

6. S. S. Chen, A. L. Moore, W. W. Cai, J. W. Suk, J. H. An, C. Mishra, C. Amos, C. W. Magnuson, J. Y. Kang, L. Shi and R. S. Ruoff, *Acs Nano*, 2011, **5**, 321-328.

7. J. H. Seol, I. Jo, A. L. Moore, L. Lindsay, Z. H. Aitken, M. T. Pettes, X. S. Li, Z. Yao, R. Huang, D. Broido, N. Mingo, R. S. Ruoff and L. Shi, *Science*, 2010, **328**, 213-216.

8. K. Yoon, G. Hwang, J. Chung, O. Kwon, K. D. Kihm and J. S. Lee, *Carbon*, 2014, **76**, 77-83.

9. S. S. Chen, Q. Y. Li, Q. M. Zhang, Y. Qu, H. X. Ji, R. S. Ruoff and W. W. Cai, *Nanotechnology*, 2012, **23**, 365701.

10. L. Lindsay, D. A. Broido and N. Mingo, *Phys. Rev. B*, 2010, **82**, 115427.

11. D. L. Nika, E. P. Pokatilov and A. A. Balandin, *Phys. Status Solidi B-Basic Solid State Phys.*, 2011, **248**, 2609-2614.

12. A. Alofi and G. Srivastava, *J. Appl. Phys.*, 2012, **112**, 013517.

13. Z. Aksamija and I. Knezevic, *Appl. Phys. Lett.*, 2011, **98**, 141919.

14. W. R. Zhong, M. P. Zhang, B. Q. Ai and D. Q. Zheng, *Appl. Phys. Lett.*, 2011, **98**, 113107.

15. D. L. Nika and A. A. Balandin, *J. Phys. Condens. Matter*, 2012, **24**, 233203.

16. X. Xu, L. F. Pereira, Y. Wang, J. Wu, K. Zhang, X. Zhao, S. Bae, C. T. Bui, R. Xie and J. T. Thong, *Nat. commun.* 2014, **5**, 3689.

17. K. M. F. Shahil and A. A. Balandin, *Nano Lett.*, 2012, **12**, 861-867.

18. P. Goli, S. Legedza, A. Dhar, R. Salgado, J. Renteria and A. A. Balandin, *J. Power Sources*, 2014, **248**, 37-43.

19. Z. Yan, G. X. Liu, J. M. Khan and A. A. Balandin, *Nat. Commun.* 2012, **3**, 827

20. P. Goli, H. Ning, X. Li, C. Y. Lu, K. S. Novoselov and A. A. Balandin, *Nano Lett.* 2014, **14**, 1497-1503.

21. Z. Gao, Y. Zhang, Y. Fu, M. M.F. Yuen, J. Liu, *Carbon*, 2013, **61**, 342-348.

22. S. Latil, V. Meunier and L. Henrard, *Phys. Rev. B*, 2007, **76**, 201402.

23. S. Shallcross, S. Sharma and O. Pankratov, *Phys. Rev. Lett.*, 2008, **101**, 056803.

24. J. L. Dos Santos, N. Peres and A. C. Neto, *Phys. Rev. Lett.*, 2007, **99**, 256802.

25. P. Poncharal, A. Ayari, T. Michel and J.-L. Sauvajol, *Phys. Rev. B*, 2008, **78**, 113407.

26. J. Hass, F. Varchon, J.-E. Millan-Otoya, M. Sprinkle, N. Sharma, W. A. de Heer, C. Berger, P. N. First, L. Magaud and E. H. Conrad, *Phys. Rev. Lett.*, 2008, **100**, 125504.

27. A. Luican, G. Li, A. Reina, J. Kong, R. Nair, K. S. Novoselov, A. K. Geim and E. Andrei, *Phys. Rev. Lett.*, 2011, **106**, 126802.

28. X. S. Li, C. W. Magnuson, A. Venugopal, R. M. Tromp, J. B. Hannon, E. M. Vogel, L. Colombo and R. S. Ruoff, *J. Am. Chem. Soc.*, 2011, **133**, 2816-2819.

29. X. S. Li, Y. W. Zhu, W. W. Cai, M. Borysiak, B. Y. Han, D. Chen, R. D. Piner, L. Colombo and R. S. Ruoff, *Nano Lett.*, 2009, **9**, 4359-4363.

30. P. Blake, E. W. Hill, A. H. C. Neto, K. S. Novoselov, D. Jiang, R. Yang, T. J. Booth and A. K. Geim, *Appl. Phys. Lett.*, 2007, **91**, 63124.

31. A. C. Ferrari, J. C. Meyer, V. Scardaci, C. Casiraghi, M. Lazzeri, F. Mauri, S. Piscanec, D. Jiang, K. S. Novoselov, S. Roth and A. K. Geim, *Phys. Rev. Lett.*, 2006, **97**, 187401.

32. C. Casiraghi, A. Hartschuh, H. Qian, S. Piscanec, C. Georgi, A. Fasoli, K. S. Novoselov, D. M. Basko and A. C. Ferrari, *Nano Lett.*, 2009, **9**, 1433-1441.

33. J. C. Meyer, A. K. Geim, M. I. Katsnelson, K. S. Novoselov, T. J. Booth and S. Roth, *Nature*, 2007, **446**, 60-63.

34. J. Bao, S. Xing, Y. Wang, W. Wu, F. Robles-Hernandez, S. pei, *Proceedings of SPIE*, 2013, **8725**, 872503.

35. R. R. Nair, P. Blake, A. N. Grigorenko, K. S. Novoselov, T. J. Booth, T. Stauber, N. M. R. Peres and A. K. Geim, *Science*, 2008, **320**, 1308-1308.

36. S. S. Chen, W. W. Cai, R. D. Piner, J. W. Suk, Y. P. Wu, Y. J. Ren, J. Y. Kang and R. S. Ruoff, *Nano Lett.*, 2011, **11**, 3519-3525.

37. S. S. Chen, Q. Z. Wu, C. Mishra, J. Y. Kang, H. J. Zhang, K. J. Cho, W. W. Cai, A. A. Balandin and R. S. Ruoff, *Nat. Mater.* 2012, **11**, 203-207.

38. J. L. dos Santos, N. Peres and A. C. Neto, *Phys. Rev. B*, 2012, **86**, 155449.

39. A. I. Cocemasov, D. L. Nika and A. A. Balandin, *Phys. Rev. B*, 2013, **88**, 035428.

40. D. L. Nika, A. I. Cocemasov and A. A. Balandin, 2014, *arXiv preprint arXiv:1405.2372*.

41. J. M. Ziman, *Electrons and phonons: the theory of transport phenomena in solids*, Oxford University Press, 2001.

42. A. Alofi and G. Srivastava, *Phys. Rev. B*, 2013, **87**, 11, 5421.

43. D. L. Nika, A. S. Askerov and A. A. Balandin, *Nano Lett.*, 2012, **12**, 3238-3244.

CAPTIONS

Figure 1: (a) Optical micrograph of bilayer graphene film on a 300 nm SiO_2/Si substrate. (b) Raman spectra of graphene measured at the positions labeled by the colored circles in (a). (c) Raman maps of the bilayer graphene areas indicated in (a). Three Raman maps, from left to right, show the integrated intensity of the G peak, the 2D peak and the FWHM of 2D peak, respectively.

Figure 2: (a) Micro-Raman 2D peak (2620-2780 cm^{-1}) map of the suspended graphene on the Au-coated SiN_x porous membrane. (b) Typical Raman spectra acquired at three different positions as marked in (a). (c-e) The selected area electron diffraction (SAED) patterns taken from three arrow labeled holes as signed in (a). (f-g) Profile plots of the diffraction peak intensities along the red and purple lines in (c) and (d). (h) Intensity profiles along AA' and BB' in (e).

Figure 3: Temperature dependence of the 2D peak spectral position as a function of temperature for single layer graphene, Bernal stacked bilayer graphene, and twisted bilayer graphene.

Figure 4: Thermal conductivity of the suspended single layer graphene, Bernal stacked bilayer graphene and twisted bilayer graphene as the function of the measured temperature. The thermal conductivity of the wrinkled single layer graphene is shown for comparison from Ref. (9).

Figure 5: (a-b) Brillouin zone and calculated phonon dispersions for Bernal stacked bilayer graphene. (c-d) Brillouin zone and calculated phonon dispersion for twisted bilayer graphene. The twist angle in the calculation was assumed to be 32.2°, which is close to the experimental value. Note the substantial reduction of the Brillouin zone in T-BLG and corresponding emergence of numerous folded phonon branches. The normal decay of the phonon with $\omega = 900\,\mathrm{cm}^{-1}$ (blue point) into two phonons with $\omega' = 800\,\mathrm{cm}^{-1}$ and $\omega'' = 100\,\mathrm{cm}^{-1}$ (green points) in T-BLG is schematically shown in (d). Note that this decay process is not allowed by the momentum conversation law in AB-BLG (b).

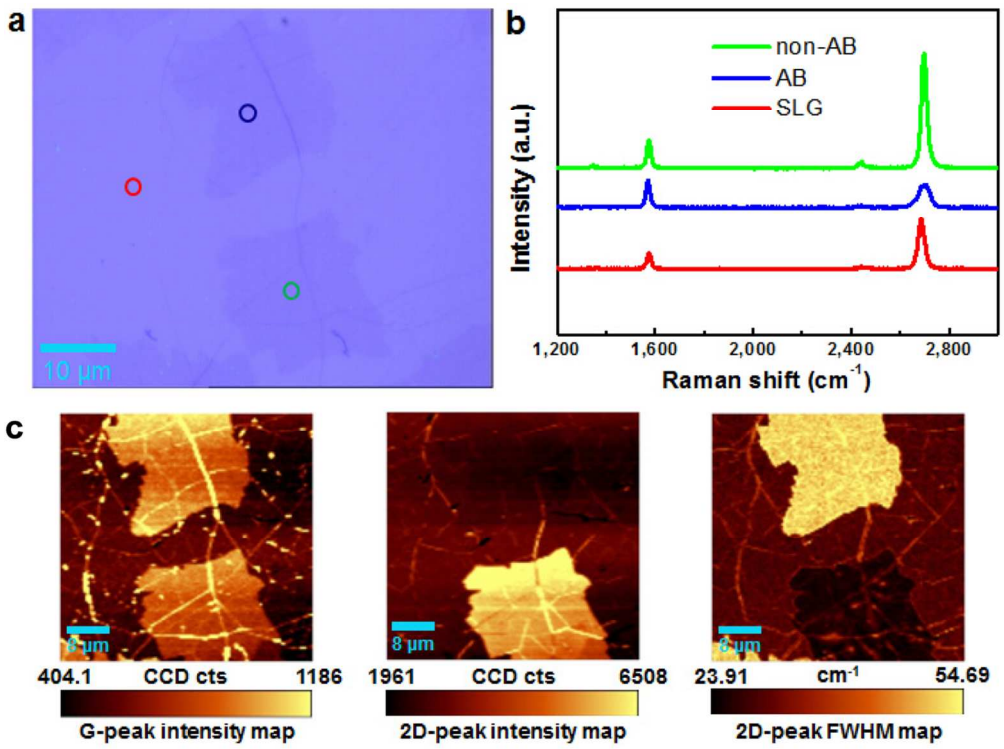

404x301mm (96 x 96 DPI)

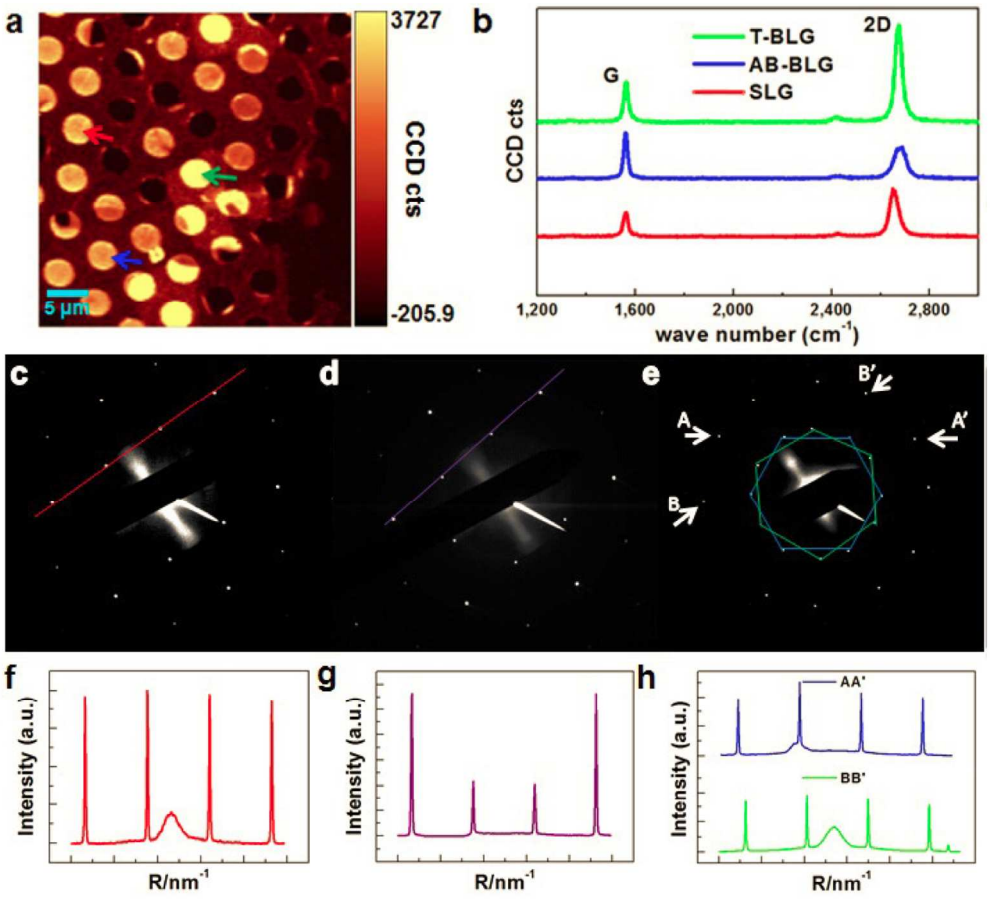

401x358mm (96 x 96 DPI)

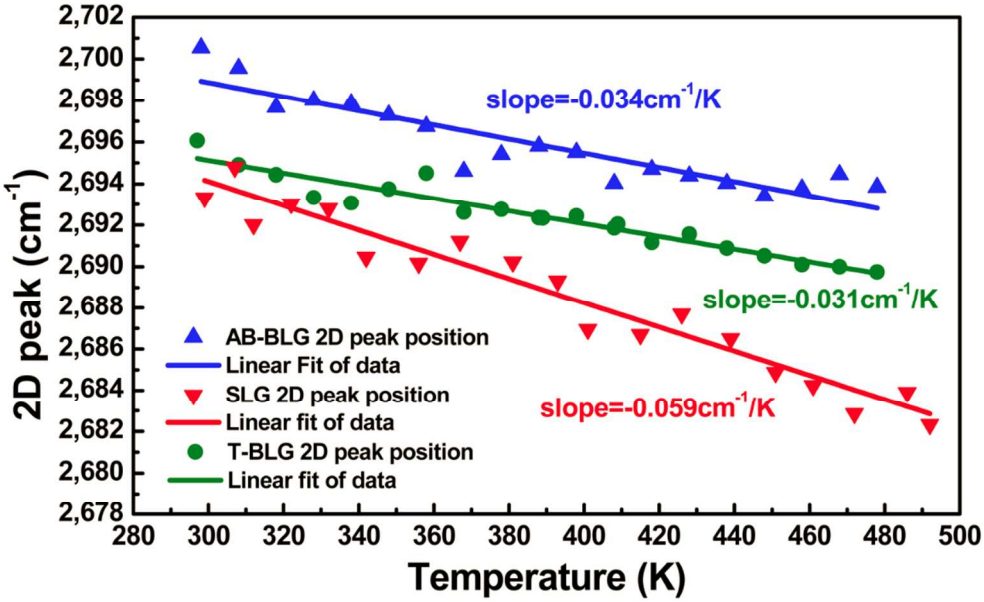

311x188mm (96 x 96 DPI)

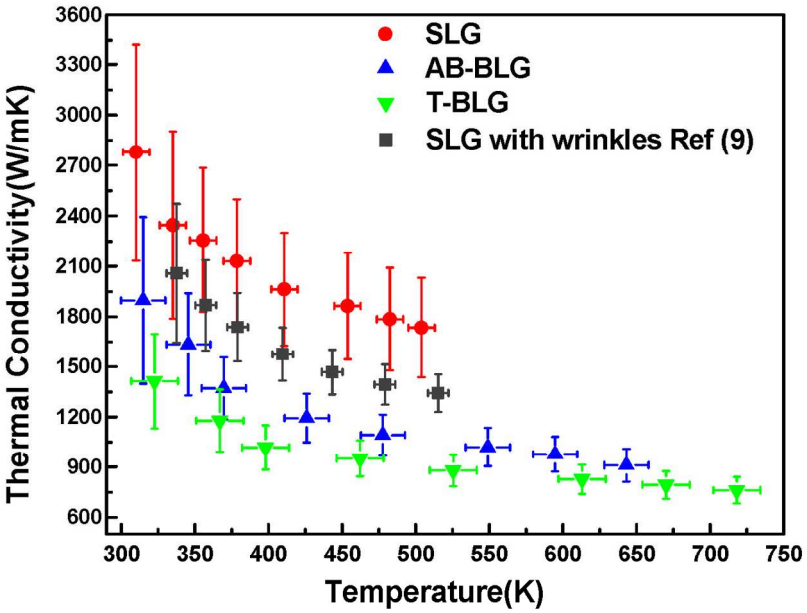

297x210mm (150 x 150 DPI)